

Advances in Electronic Ceramics

Ceramic Engineering and Science Proceedings
Volume 28, Issue 8

Edited by

Clive Randall

Hua-Tay Lin

Kunibito Koumoto

Paul Clem

Volume Editors

Jonathan Salem

Dongming Zhu

Thermoelectric Properties of Pb and Sr Doped $\text{Ca}_3\text{Co}_4\text{O}_9$ Hiroshi Nakatsugawa, Hyeon Mook Jeong, Natsuko Gomi, Hiroshi Fukutomi, and Rak Hee Kim	171
Thermoelectric Properties of Mix-Crystal Compound $\text{Mg}_2\text{Si-Mg}_3\text{Sb}_2$ Dongli Wang and G.S. Nolas	185
Thermoelectric Performance of Doped $\text{SrO}(\text{SrTiO}_3)_n$, ($n = 1, 2$) Ruddlesden-Popper Phases Kyu Hyoung Lee, Yi Feng Wang, Hiromichi Ohta, and Kunihito Koumoto	193
Growth of $\text{Bi}_2\text{Ca}_2\text{Co}_{1.69}\text{O}_x$ Cobaltite Rods by Laser Floating Zone Method E. Guilmeau, A. Sotelo, M.A. Madre, D. Chateigner, and D. Grebille	203
Growth and Characterization of Germanium-Based Type I Clathrate Thin Films Deposited by Pulsed Laser Ablation Robert Hyde, Matt Beekman, George S. Nolas, Pritish Mukherjee, and Sarath Witanachchi	211
Synthesis and Characterization of Chalcogenide Nanocomposites J. Martin and G.S. Nolas	221
Anomalous Thermal Conductivity Observed in the $\text{Na}_{1-x}\text{Mg}_x\text{V}_2\text{O}_6$ Single Crystals Z. Su, J. He, and T. M. Tritt	227
Physical Properties of Hot-Pressed $\text{K}_8\text{Ge}_4\text{□}_2$ M. Beekman and G.S. Nolas	233
TRANSPARENT ELECTRONIC CERAMICS	
Advanced Indium Tin Oxide Ceramic Sputtering Targets and Transparent Conductive Thin Films Eugene Medvedovski, Neil A. Alvarez, Christopher J. Szepesi, Olga Yankov, and Maryam K. Olsson	243
Author Index	257

GROWTH OF $\text{Bi}_2\text{Ca}_2\text{Co}_{1.69}\text{O}_x$ COBALTITE RODS BY LASER FLOATING ZONE METHOD

E. Guilmeau,¹ A Sotelo,² M. A. Madre,² D. Chateigner,¹ and D. Grebille¹

¹CRISMAT Laboratory, UMR 6508 CNRS-ENSICAEN. 6 Bd Maréchal Juin. 14050 CAEN cedex, E-mail: emmanuel.guilmeau@ensicaen.fr

²Instituto de Ciencia de Materiales de Aragón (UZ-CSIC). Dpto. Ciencia y Tecnología de Materiales y Fluidos. C/M^a de Luna, 3. 50018 Zaragoza

ABSTRACT

This paper reports the synthesis and characterization of Bi-based misfit cobaltite rods. The specimens have been processed through the Laser Floating Zone method in air. The electrical resistivity (ρ) of directionally solidified rods were determined and correlated with the textural and microstructural features (neutron diffraction and scanning electron microscopy). This work is the first step of our researches in the field of Bi-cobaltite as-synthesized by the Laser Floating Zone method, and gives an interesting approach with the view to engineering their properties and synthesizing other promising thermoelectric compounds.

1. INTRODUCTION

Since the discovery of large thermoelectricity in Na_xCoO_2 ,¹ enthusiastic efforts have been devoted to explore new Co oxides exhibiting high thermoelectric performances, and some layered cobaltites, such as $[\text{Ca}_2\text{CoO}_3][\text{CoO}_2]_{1.62}$ and $[\text{Bi}_{0.87}\text{SrO}_2]_2[\text{CoO}_2]_{1.82}$ were found to exhibit good thermoelectric (TE) properties as well.²⁻⁴

The crystal structure of these layered cobaltites is composed of an alternate stacking of a common conductive CdI_2 -type CoO_2 layer with a two-dimensional triangular lattice and a block layer, composed of one (in Na_xCoO_2) to several insulating rock-salt-type (RS) layer (in $[\text{Bi}_{0.87}\text{SrO}_2]_2[\text{CoO}_2]_{1.82}$ or $[\text{Bi}_{0.81}\text{CaO}_2]_2[\text{CoO}_2]_{1.69}$)⁵⁻⁷. Derived from Na_xCoO_2 , the structure of these cobalt oxides consist of single hexagonal CoO_2 layers stacked with quadruple rock-salt layers composed of double [Bi-O] and [Ca-O] layers. The two RS and CoO_2 layers have common a and c axes, while the b -axis lengths of the two layers are different. Due to their high structural anisotropy, the alignment of plate-like grains by mechanical and/or chemical processes is necessary to attain macroscopic properties comparable to the intrinsic crystallographic ones. The preferential grain orientation is expected to improve the transport properties of the bulk material and to reach, if possible, the TE properties of the single crystal. Here is reported the processing of long textured Bi-based cobaltite bulk ceramics by the laser floating zone (LFZ) technique⁸⁻⁹. Long lengths (more than 25 cm) of textured materials have been processed. The microstructural characterization of the textured ceramics has been performed by scanning electron microscopy (SEM), and the texture was determined by neutron diffraction.

2. EXPERIMENTAL

Polycrystalline ceramics with the initial composition $\text{Bi}_2\text{Ca}_2\text{Co}_{1.7}\text{O}_x$, $\text{Bi}_2\text{Sr}_2\text{Co}_{1.8}\text{O}_x$, and $\text{Bi}_2(\text{Ca,Sr})_2\text{Co}_{1.75}\text{O}_x$ were prepared by the conventional solid-state synthesis technique from

commercial Bi_2O_3 (Panreac, 98 + %), SrCO_3 (Panreac, 98 + %), CaCO_3 (Panreac, 98.5 + %) and Co_2O_3 (Aldrich, 98 + %) powders.

These powders were weighed in the adequate proportions, mixed, milled in an agate ball mill for 30 minutes at 60 rpm, and calcined at 750°C for 12 h in air to assure the carbonates decomposition. The resulting powder was then carefully ground in an agate mortar, followed by a ball milling for 30 minutes at 60 rpm to assure good homogeneity of the mixture. The obtained product was then introduced in a furnace at 800°C for 12 h in air, reground and ball milled to obtain a fine powder, which was isostatically pressed at 200 MPa in order to obtain green ceramic cylinders. These cylinders have been then heated at 800°C for several hours, and quenched at room temperature in air, to improve their mechanical properties as they have to be used as feed in a LFZ device⁸ equipped with a power Nd:YAG continuous laser (1.06 μm). The growth was performed downwards at growth rates of 15, 30 and 50 mm/h for each composition, with a relative rotation, between feed and seed, of 15 rpm, leading to long (more than 25 cm) and textured cylindrical rods.

The texture of the hot-forged sample was determined from neutron diffraction spectra. For that purpose, the cylindrical rod was cut in several pieces of 10 mm in length. They were paste ones beside the others to form an approximate rod of 10 mm in diameter and 10 mm in length. With this almost symmetric configuration, the whole volume of the sample is analyzed by the neutron beam. A curved position-sensitive detector coupled to a tilt angle (χ) scan allowed the whole diffraction pattern treatment in the combined Rietveld-WIMV algorithm, implemented in the MAUD software.¹⁰⁻¹¹ X-ray structural determination performed on the single crystal¹² was used to describe the 3D structural model of the $[\text{Bi}_{0.81}\text{CaO}_2]_2[\text{CoO}_2]_{1.69}$ phase in the MAUD software using the supercell description, and to determine through an iterative methodology the texture of the cobaltite. Experiments were carried out on the D1B neutron line at the Institut Laue Langevin, Grenoble. The neutron wavelength is monochromatised to $\lambda=2.523$ Å. Diffracted neutrons are collected on a 80° (resolution 0.2°) 2 θ range. Scans for combined analysis were operated from $\chi = 0$ to 90° (step 5°) using a fixed incidence angle ω of 25.11°. The average volume of the sample is 100 mm³, and the measuring times were around 20 min per sample orientation.

Electrical resistivity measurements were performed by the standard dc four-probe technique from 5 to 400K at self field in a Physical Properties Measurement System (PPMS) from Quantum Design. The scanning electron microscopy (SEM) observations were made using a Zeiss Supra 55.

3. RESULTS AND DISCUSSION

The figure 1 illustrates three different $\text{Bi}_2\text{Ca}_2\text{Co}_{1.7}\text{O}_x$ grown bars according to their initial green shapes before the translating growth (50 mm/h). It evidences the potential of the technique to grow cylindrical rods with diameters of several millimeters.



Figure 1: $\text{Bi}_2\text{Ca}_2\text{Co}_{1.7}\text{O}_x$ grown rods depending of their initial green shapes before the translating growth (50 mm/h).

The figure 2 shows the transversal fracture along the bar axis. It can be clearly identified that the grains grow preferentially parallel to the cylindrical axis whereas an initial angle growth of around 30° is observed. In figure 2b, a close view of the fracture shows large platelike grains, with dimensions of several hundred of micrometers in the ab planes, and several micrometers in the c direction. As speculated from the microstructures, the texture (*i.e.* the c -axes of the misfit structure are preferentially aligned perpendicular to the rod axis) has been attested by neutron diffraction.

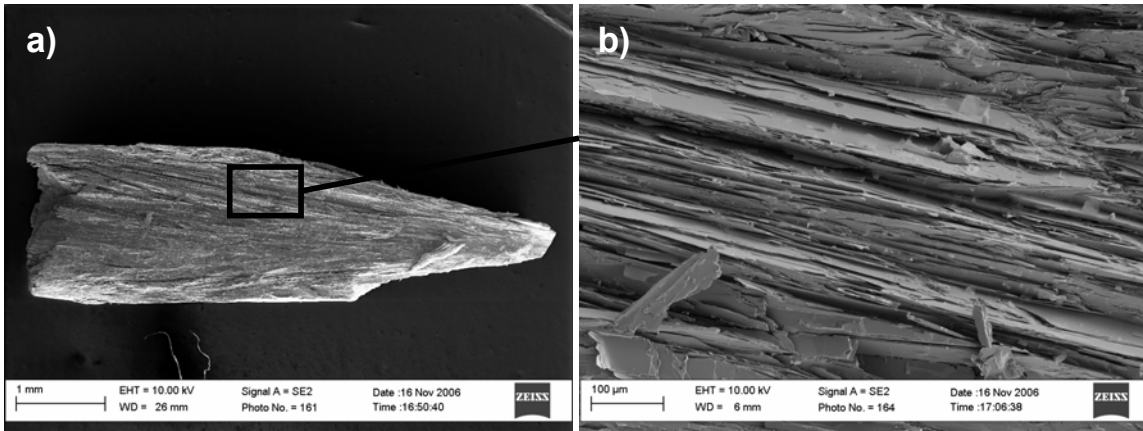


Figure 2: SEM micrographies of (a) a transversal fracture along the rod axis and (b) a close view showing the large platelike grains. $\text{Bi}_2\text{Ca}_2\text{Co}_{1.7}\text{O}_x$ compound.

The figure 3 presents the measured neutron diffraction pattern for all χ orientations of the sample. Firstly, it can be clearly seen that major peaks correspond to the misfit cobaltite $\text{Bi}_2\text{Ca}_2\text{Co}_{1.7}\text{O}_x$ whose the general monoclinic structure is described by two sublattices with their different b parameters: $a=4.90\text{\AA}$, $b_1=4.73\text{\AA}$, $b_2=2.80\text{\AA}$, $c=14.66\text{\AA}$, $\beta=93^\circ49'$.¹² Secondly, this graph highlights without ambiguity the texture. In particular, we clearly observe the intensity decrease of the $(hk0)$ peaks when χ increases and the appearance of the $(00l)$ peaks when χ tends to 90° .

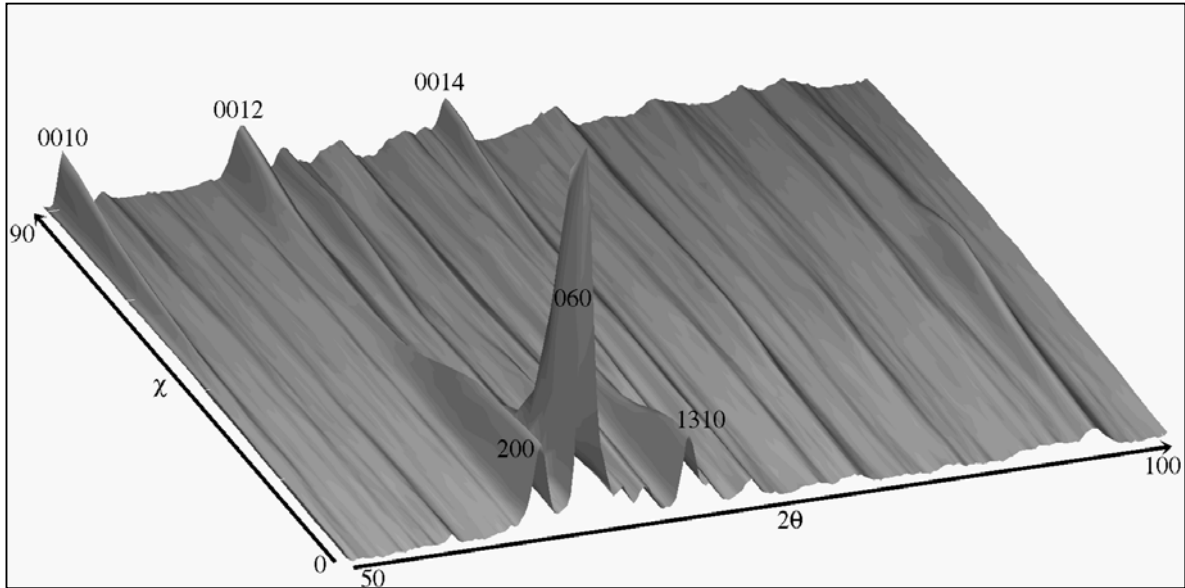


Figure 3: Neutron diffraction pattern operated for 19 χ -scans from $\chi = 0$ to 90° (step 5°) using a fixed incidence angle ω of 25.11° ($\{006\}$ Bragg position).

Based on a 3D structural model, reconstructed from the single crystal data, the whole diffraction pattern was refined. In figure 4, we can visually appreciate the agreement between the experimental (dots) and refined (lines) spectra for all the χ orientations. The refinement reliability is established by RP_0 , RP_1 for the Orientation Distribution (OD) refinement, and R_w and RB factors for the Rietveld data, equal to 9.5%, 7.1 %, 9.6%, and 4.2%, respectively.

Figure 5 shows the inverse pole figures calculated for the z fiber direction, parallel to the translation axis. It shows a preferential orientation of the a and b-axis along the translation direction. Whereas we were attending a symmetric planar texture, with an equivalent orientation of the $[hk0]$ direction along the translation axis, the results show that the melting zone has induced a preferential growth of the platelike grains along some precise directions.

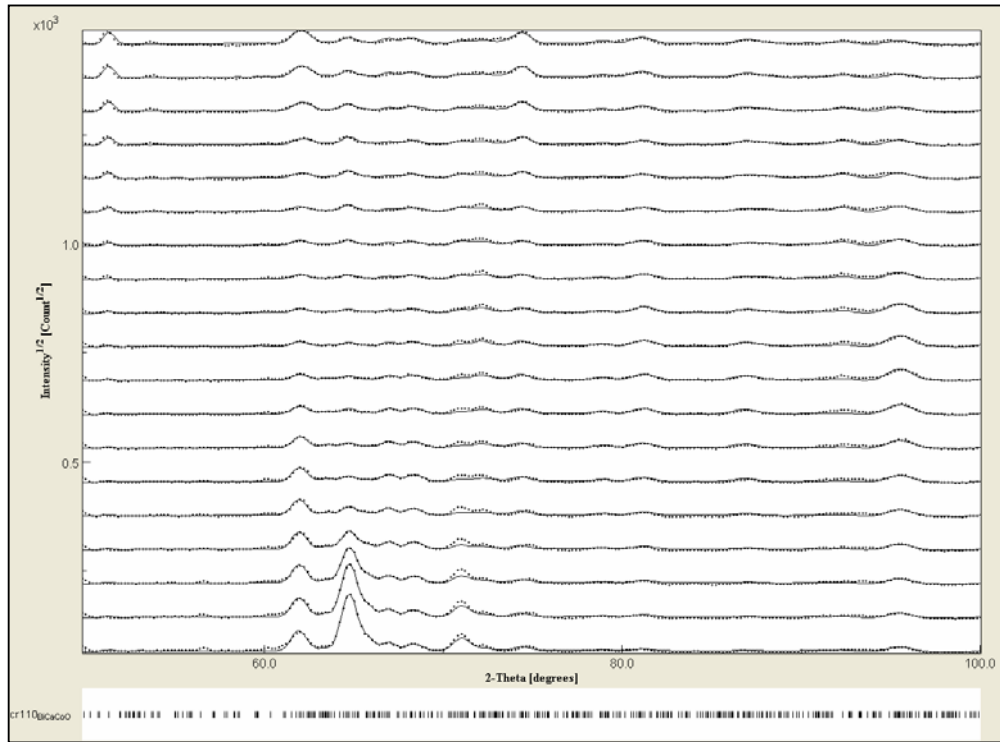


Figure 4: Experimental (dots) and calculated (lines) neutron diffraction patterns for various χ positions (0 to 90°).

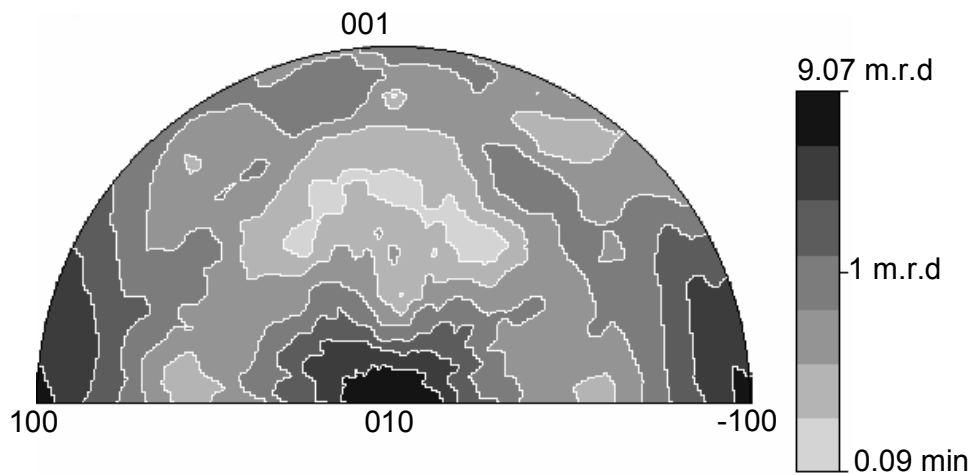


Figure 5: Inverse pole figures calculated for the z direction, parallel to the hot-forging direction.

In terms of thermoelectric properties, at that time, only electrical resistivity measurements have been performed. These ones are presented in figure 6. According to the literature,¹³⁻¹⁴ the

cylindrical rods, synthesized from the $\text{Bi}_2\text{Sr}_2\text{Co}_{1.8}\text{O}_x$ composition, exhibit a semiconductor/metal transition around 100-150K, whatever the translation speed growth is. On the opposite, the $\text{Bi}_2\text{Ca}_2\text{Co}_{1.7}\text{O}_x$ and $\text{Bi}_2(\text{Ca,Sr})_2\text{Co}_{1.75}\text{O}_x$ compositions exhibit a semiconducting behavior on the full range of temperature, according to our last study on the BiCaCoO system.¹⁵ As a general trend, *i.e.* for the three compositions, the translation speed has a significant influence on the transport properties. The decreasing up to 15 mm/h allows a reduction of the resistivity by a factor 1.5-2, whatever the composition is. This indicates that the crystal growth has an impact on the texturation and consequently on the transport behavior. Actually, we have not all the data to argue our hypothesis, but we strongly believe that the texture strength, the density and the crystallite size are the major factors of the electrical resistivity variations.

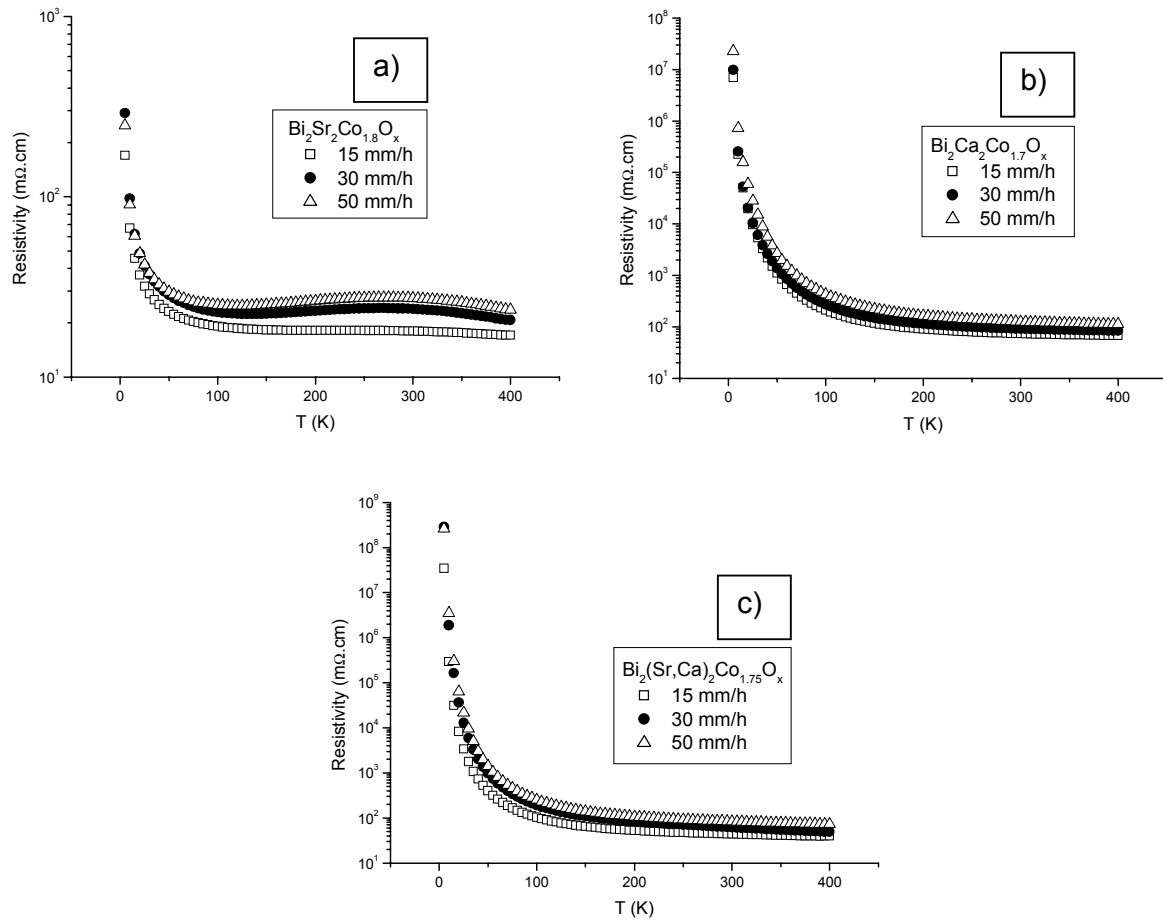


Figure 6: Resistivity versus temperature curves, for the (a) $\text{Bi}_2\text{Ca}_2\text{Co}_{1.7}\text{O}_x$, (b) $\text{Bi}_2\text{Sr}_2\text{Co}_{1.8}\text{O}_x$, and (c) $\text{Bi}_2(\text{Ca,Sr})_2\text{Co}_{1.75}\text{O}_x$ compositions, depending of the LFZ translation speed.

Finally, the figure 7 presents the resistivity versus temperature curves of the three compositions for a fixed LFZ translation speed of 15 mm/h. The magnitude of the resistivity is

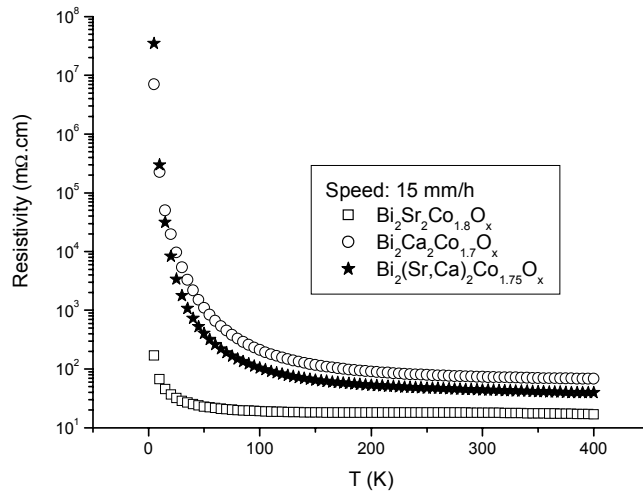


Figure 7: Resistivity versus temperature curves, for the three compositions. LFZ translation speed = 15 mm/h.

reduced by modifying the alkaline earth cations, which indicates and confirms¹⁶ that the increase of the ionic radius of the alkaline earth cations induces an increase of the misfit ratio, thereby resulting in increasing the Co ions valence in the CoO₂ layer and consequently increasing the carrier concentration. For confirming this hypothesis, thermopower measurements will be carried out soon.

4. CONCLUSIONS

Preliminary results highlight the reliability and effectiveness of the LFZ method for texturing Bi-based misfit cobaltite rods. Neutron diffraction evidenced the texture developed during the melting growth. The electrical resistivity measurements of the three studied compounds, *i.e.* Bi₂Ca₂Co_{1.7}O_x, Bi₂Sr₂Co_{1.8}O_x, and Bi₂(Ca,Sr)₂Co_{1.75}O_x, depending of the translation speed, are in agreement with the results reported in the literature. Other physical properties characterizations (thermopower, thermal conductivity) are now under investigation in order to check the role of the composition and microstructure on the transport properties.

REFERENCES

- 1) I. Terasaki, Y. Sasago, and K. Uchinokura, Phys. Rev. B 1997, 56, R12685.
- 2) R. Funahashi, I. Matsubara, H. Ikuta, T. Takeuchi, U. Mizutani, and S. Sodeoka, Jpn. J. Appl. Phys. 2000, 39 L1127.
- 3) A.C. Masset, C. Michel, A. Maignan, M. Hervieu, O. Toulemonde, F. Studer, B. Raveau, and J. Hejtmanek, Phys. Rev. B 2000, 62, 166.
- 4) H. Leligny, D. Grebille, O. Perez, A. C. Masset, M. Hervieu, and B. Raveau, Acta Cryst. B 2000, 56, 173.
- 5) A. Maignan, S. Hébert, M. Hervieu, C. Michel, D. Pelloquin, and D. Khomskii, J. Phys.: Condens. Matter. 2003, 15, 2711.
- 6) H. Itahara, C. Xia, J. Sugiyama, and T. Tani, Chem. Mater., 2004, 14, 61.

- 7) E. Guilmeau, M. Mikami, R. Funahashi, and D. Chateigner, *J. Mater. Res.* 2005, 20, 1002.
- 8.- G. F. de la Fuente, J. C. Diez, L. A. Angurel, J. I. Peña, A. Sotelo, R. Navarro, *Adv. Mater.*, 1995, 7, 853.
- 9.- Y. Huang, G. F. de la Fuente, A. Sotelo, A. Badía, F. Lera, R. Navarro, C. Rillo, R. Ibáñez, D. Beltran, F. Sapiña, A. Beltran, *Physica C*, 1991, 185, 2401.
- 10) L. Lutterotti, S. Matthies, H. R. Wenk, *Proceedings of the 12th International Conference on Textures of Materials*, Vol. 2, edited by J. A. Szpunar, 1999, 1599-1604. Montreal: NRC Research Press., Freeware available at: <http://www.ing.unitn.it/~luttero/maud/>
- 11) E. Guilmeau, D. Chateigner, J. Noudem, R. Funahashi, S. Horii, and B. Ouladdiaf, *J. Appl. Cryst.* 2005, 38, 199.
- 12) D. Grebille, H. Muguerra, E. Guilmeau, H. Rousselière, and R. Cloots, *Chem. Mater.* (Submitted)
- 13) T. Fujii and I. Terasaki, *cond.mat.* 2002, 0210071, New thermoelectric Materials Workshop: Beyond Bismuth Telluride”.
- 14) T. Yamamoto, K. Uchinokura, and I. Tsukada, *Phys. Rev. B* 2002, 65, 184434.
- 15) E. Guilmeau, M. Pollet, D. Grebille, M. Hervieu, H. Muguerra, R. Cloots, M. Mikami, and R. Funahashi, *Inorg. Chem.* 46 (2007) 2124.
- 16) H. Itahara, C. Xia, J. Sugiyama, and T. Tani, *Journal of Materials Chemistry*, 2004, 14, 61